Donor–Acceptor Systems

International Edition: DOI: 10.1002/anie.201601672
German Edition: DOI: 10.1002/ange.201601672

Construction of an Artificial Ferrimagnetic Lattice by Lithium Ion Insertion into a Neutral Donor/Acceptor Metal–Organic Framework

Kouji Taniguchi, Keisuke Narushima, Julien Mahin, Wataru Kosaka, and Hitoshi Miyasaka**

Abstract: *Construction of a molecular system in which the magnetic lattice exhibits long-range order is one of the fundamental goals in materials science. In this study, we demonstrate the artificial construction of a ferrimagnetic lattice by doping electrons into acceptor sites of a neutral donor/acceptor metal–organic framework (D/A-MOF). This doping was achieved by the insertion of Li-ions into the D/A-MOF, which was used as the cathode of a Li-ion battery cell. The neutral D/A-MOF is a layered system composed of a carboxylate-bridged paddlewheel-type diruthenium(II,II) complex as the donor and a TCNQ derivative as the acceptor. The ground state of the neutral form was a magnetically disordered paramagnetic state. Upon discharge of the cell, spontaneous magnetization was induced; the transition temperature was variable. The stability of the magnetically ordered lattice depended on the equilibrium electric potential of the D/A-MOF cathode, which reflected the electron-filling level.*

Over the past few decades, the design of molecule-based magnets with long-range magnetic order has attracted much interest in the field of molecular functional materials.[1] One route to achieve such long-range magnetic order is to construct lattices using only paramagnetic metal ions and/or molecules with the help of superexchange coupling between paramagnetic centers via a bridging ligand. Charge-transfer (CT) framework systems comprising electron donor (D) and electron acceptor (A) units are fascinating candidates for such molecule-based magnets because energetically controlled electron transfer (ET) from D^0 to A^0 causes unpaired electron spins in both ionized units, D^+ and A^-, strongly magnetically coupled with the mediation of CT between D^+ and A^-.[1,2] We have previously demonstrated such CT/ET-dependent magnetic behavior in a family of D/A metal–organic frameworks (D/A-MOFs) with a D_2A formulation composed of carboxylate-bridged paddlewheel-type diruthenium(II,II) complexes ($[Ru_2^{II,II}]$) as D and 7,7,8,8-tetracyano-*p*-quinodimethane (TCNQ) derivatives as A; long-range magnetic order was observed only in the one-electron transferred ionic state ($D^{0.5+}{}_2A^-$) containing the $A^{\bullet-}$ radical form ($TCNQ^{\bullet-}$).[3] Thus, in the case of the neutral state of the above-mentioned D/A-MOFs (that is, $D^0{}_2A^0$), the key factor required to induce long-range magnetic order is the generation of the radical $A^{\bullet-}$ vs. paramagnetic D^0 (that is, $[Ru_2^{II,II}]$) with $S=1$ (Figure 1). In fact, a layered framework with the $D^0{}_2A^{\bullet-}$ charge state displayed a strong magnetic correlation between the spins of D^0 and $A^{\bullet-}$, which finally underwent long-range magnetic ordering at $T_C=82$ K by combining with an $S=1/2$ spin of $[FeCp^*{}_2]^+$ located between layers.[4]

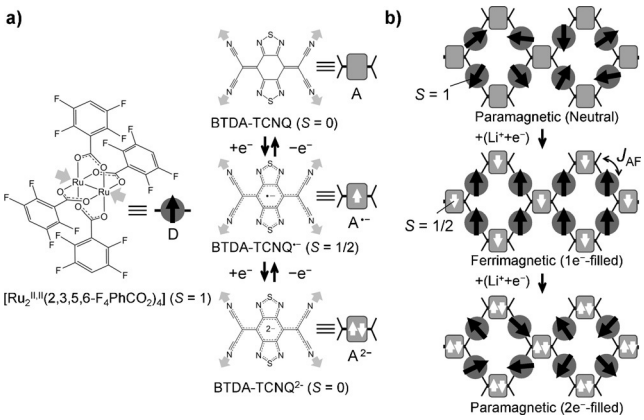

Figure 1. a) Representations of $[Ru_2^{II,II}(2,3,5,6\text{-}F_4PhCO_2)_4]$ ($S=1$) as a donor (D) and BTDA-TCNQ as an acceptor (A) with its redox forms of BTDA-TCNQ ($S=0$), $BTDA\text{-}TCNQ^{\bullet-}$ ($S=1/2$) and $BTDA\text{-}TCNQ^{2-}$ ($S=0$). b) Plausible spin ordered states produced by electron-filling of A with Li^+-ion insertions into a neutral state (**1′**), where neutral, 1 e^--filled, and 2 e^--filled forms are expected to be paramagnetic, ferrimagnetic, and paramagnetic, respectively.

Focusing on the generation of the radical $A^{\bullet-}$ in the $D^0{}_2A^0$ system, electron-filling control of the system should be an effective approach for the construction of an artificial magnetically ordered lattice without intra-lattice ET. Taking into account that the present "MOFs" are also characterized as a type of porous frameworks, the electrochemical insertion of ionic guests such as Li^+ and Na^+ into host frameworks is potentially applicable for electron-filling control of D/A-MOFs.[5] In the process of electrochemical cation insertion, a cation and electron pair is introduced into the host material and the valence of the redox-active species (that is, the acceptor A^0) in the material is directly modulated from A^0

[*] Dr. K. Taniguchi, K. Narushima, J. Mahin, Dr. W. Kosaka, Prof. Dr. H. Miyasaka
Institute for Materials Research (IMR), Tohoku University
2-1-1 Katahira, Aoba-ku, Sendai, 980-8577 (Japan)
and
Department of Chemistry, Graduate School of Science
Tohoku University
6-3 Aramaki-Aza-Aoba, Aoba-ku, Sendai 980–8578 (Japan)
E-mail: taniguchi@imr.tohoku.ac.jp
miyasaka@imr.tohoku.ac.jp
J. Mahin
Institute of Condensed Matter and Nanosciences, Molecules, Solids and Reactivity (IMCN/MOST), Université Catholique de Louvain
Place Louis Pasteur 1, 1348 Louvain-la-Neuve (Belgium)

Supporting information for this article can be found under: http://dx.doi.org/10.1002/anie.201601672.

to A^- or A^{2-} accompanied by charge compensation by the introduced cation species (Figure 1a).[5b] Several compounds with redox-active components, such as a Prussian blue analogue,[6] octacyanometallate-bridged coordination polymers,[7] and transition-metal oxides,[8] have been magnetically manipulated by electrochemical ion insertion and subsequent valence control of the transition metal ions; however, these reports have all been limited to the modification of magnetically pre-ordered states. We report the development of long-range magnetic ordering from a paramagnetic ground state by electron-filling control involving electrochemical ion insertion. A neutral D/A-MOF containing redox-active component is proposed as a nice playground for the construction of artificial magnetic lattice (Figure 1b).

In the $[Ru_2]$/TCNQ-MOF system, the energy difference between the highest-occupied molecular orbital (HOMO) level of D and the lowest-unoccupied molecular orbital (LUMO) level of A, $\Delta E_{H-L}(DA) \equiv E_{LUMO}(A) - E_{HOMO}(D)$, can be used to predict the electronic state, as $\Delta E_{H-L}(DA) > 0$ for the neutral state and $\Delta E_{H-L}(DA) < 0$ for the ionic state.[9–11] The HOMO and LUMO levels can be simply calculated using the density functional theory.[9–13] Following this rule, a D/A set of $[Ru_2^{II,II}(2,3,5,6\text{-}F_4PhCO_2)_4(THF)_2]$ with $E_{HOMO}(D) = -4.8518$ eV[14] and bis(1,2,5-thiadiazolo)tetracyanoquinodimethane (BTDA-TCNQ) with $E_{LUMO}(A) = -4.7353$ eV[11] (Figure 1a) was chosen because, in this case $\Delta E_{H-L}(DA) = 0.1165$ eV, which provided a new, neutral D_2A-type layered MOF, $[\{Ru_2(2,3,5,6\text{-}F_4PhCO_2)_4\}_2(BTDA\text{-}TCNQ)]\cdot 4\,CH_2Cl_2\cdot 2\,(p\text{-xylene})$ (**1**; Supporting Information, Figure S1).

Compound **1** crystallized in the triclinic space group $P\bar{1}$ (see the Supporting Information) with a formula unit comprising two $[Ru_2]$ units and one BTDA-TCNQ unit (that is, D_2A-type), in which two $[Ru_2]$ units and one BTDA-TCNQ molecule were crystallographically characterized as asymmetric units with inversion centers on the midpoint of respective units ($Z = 1$; Supporting Information, Figure S1a). The four C≡N groups of the BTDA-TCNQ unit coordinate to the axial sites of the $[Ru_2]$ units, forming a typical D_2A-type two-dimensional fishnet framework spreading parallel to the (100) plane (Supporting Information, Figure S1b,c). Compound **1** contains four CH_2Cl_2 and two molar *p*-xylene molecules per unit as crystallization solvents, which are located between D_2A layers. The *p*-xylene molecules form a π-stacking motif with the BTDA-TCNQ moieties through a [···BTDA-TCNQ···(*p*-xylene)···(*p*-xylene)···] column along the *a* axis. The oxidation states of the $[Ru_2]$ and BTDA-TCNQ units were estimated by comparing the bond lengths in the respective units with those in standard compounds (Supporting Information, Tables S1 and S2), which confirmed that **1** exists in the neutral state comprising $[Ru_2^{II,II}]$ and BTDA-TCNQ^0 units. The neutral form of **1** was also confirmed by the observation of paramagnetic behavior arising from the $S = 1$ spins of $[Ru_2^{II,II}]$ units across the temperature range 1.8–300 K (Supporting Information, Figure S2).

Even at room temperature, compound **1** easily releases the CH_2Cl_2 molecules to provide the CH_2Cl_2-free compound $[\{Ru_2(2,3,5,6\text{-}F_4PhCO_2)_4\}_2(BTDA\text{-}TCNQ)]\cdot 2\,(p\text{-xylene})$ (**1′**). The crystal sample of **1′** used in subsequent measurements was prepared by placing a sample of **1** in vacuo for approximately 12 h at room temperature. Compound **1′** is very stable at room temperature, even under vacuum; the stability of **1′** was confirmed by thermogravimetry (Supporting Information, Figure S3) and X-ray powder diffraction (XRPD) (Supporting Information, Figure S4). Finally, the structure of **1′** was determined using the combined techniques of single-crystal X-ray crystallography and the Rietveld method on XRPD.

Compound **1′** crystallized in the monoclinic space group $P2_1/n$ (Supporting Information, Supporting Information); only one $[Ru_2]$ unit and one BTDA-TCNQ molecule lying on a C_2 axis were crystallographically characterized as an asymmetric unit ($Z = 2$) (Figure 2a). The typical two-dimensional fishnet framework, which was parallel to the (10−1) plane, is maintained in **1′** (Figure 2b,c). Compound **1′** contained two molecules of *p*-xylene per unit as crystallization solvents; these were located between the MOF layers, forming the same π-stacking motif with BTDA-TCNQs as found in **1**. The volume of the void space was 182.6 Å^3, corresponding to 4.1% of the cell volume (the volume occupied by CH_2Cl_2 in **1** was 364.8 Å^3, corresponding to 15.4% of the cell volume). The oxidation state of **1′** was also estimated from the structure (Supporting Information, Tables S1 and S2); these structural characteristics confirm that the neutral state was preserved even in **1′**. Indeed, its

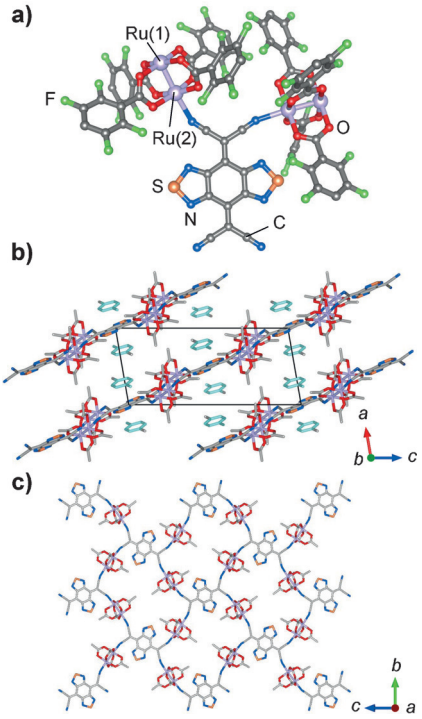

Figure 2. a) Structure of the formula unit of **1′** (solvent molecules and hydrogen atoms are omitted for clarity).[18] b) A packing form projected along the *b* axis, with the interstitial *p*-xylene solvent molecules displayed in pale blue. c) Two-dimensional D_2A layer structure in the (10−1) plane. In (b) and (c), hydrogen atoms and the 2,3,5,6-F_4Ph part of 2,3,5,6-$F_4PhCO_2^-$ are omitted for clarity.

magnetic properties agree with this conclusion (Supporting Information, Figure S5).

Electron-filling control of **1′** was performed using Li-ion insertion (Figure 1b) based on the Li-battery cell system, in which Li-metal is employed as the anode. The cathode was fabricated by mixing ground crystals of **1′** with conductive acetylene black and polytetrafluoroethylene as a binder. The prepared cathode was measured by PXRD and its identical crystallinity in discharge processes was confirmed (Supporting Information, Figure S6). The cell was assembled using lithium bis(trifluoromethylsulfonyl)amide (LiTFSA) and the *N*-methyl-*N*-propylpyrrolidinium salt of bis(fluorosulfonyl)amide (Py_{13}-FSA; ionic liquid) as electrolyte, under an Ar atmosphere.[15] During the insertion of Li-ions into **1′**, the galvanostatic intermittent titration technique (GITT) was used to suppress inhomogeneous Li-ion insertion.[16] In GITT, a low constant current (1.18 mA g^{-1}) was repeatedly applied for 1 h (discharge/charge), followed by an interval of 1 h to allow the system to reach an equilibrium state with respect to **1′**. Figure 3a shows the open-circuit voltages (OCVs) of the

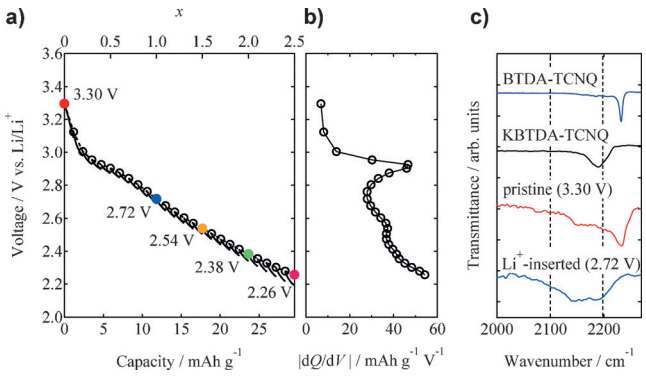

Figure 3. a) Open-circuit voltage (OCV) as a function of capacity for the cathode of $Li_x[\{Ru_2(2,3,5,6\text{-}F_4PhCO_2)_4\}_2(BTDA\text{-}TCNQ)]\cdot 2(p\text{-xylene})$ (open circles), where the solid line shows the change in voltage of the Li-battery cell during the Li^+-insertion process (discharge) at a constant current. Red and blue closed circles indicate the samples taken for IR measurements shown in (c). The *x* is the nominal Li-composition per formula unit estimated from the discharged capacity, which includes the contribution from irreversible capacity of Li-battery cell. b) Derivative of the capacity (*Q*) in (a) with respect to the voltage (*V*), d*Q*/d*V*. c) IR spectra of BTDA-TCNQ, K[BTDA-TCNQ], the cathodes of pristine (3.30 V) and Li^+-inserted compound (2.72 V), measured on KBr pellets at room temperature.

Li-battery cell, which reflect the equilibrium electrochemical potentials upon reduction of the $Li_x[\{Ru_2(2,3,5,6\text{-}F_4PhCO_2)_4\}_2(BTDA\text{-}TCNQ)]\cdot 2(p\text{-xylene})$ cathode during the Li-ion insertion process using GITT. The voltage curve shows a slope that is dependent on the capacity, which indicates that the Li-ion insertion process for **1′** is not a two-phase-coexisting reaction with a flat voltage profile,[17] which is often expected for electron localized systems (see the Supporting Information). In Figure 3b, the derivative of the capacity (*Q*) with respect to the voltage (*V*), d*Q*/d*V*, is plotted. Two peaks were observed at approximately 2.9 V and 2.4–2.7 V vs. Li/Li^+, indicating that two distinct reduction potentials exist in the discharge-voltage range between 2.2–3.4 V vs. Li/Li^+. OCV of $Li_xBTDA\text{-}TCNQ$ (Supporting Information, Figure S7) indicates two-step reductions at approximately 2.9 V and 2.4 V vs. Li/Li^+, which correspond to $A^0 \rightarrow A^{\bullet -}$ and $A^{\bullet -} \rightarrow A^{2-}$, respectively. By comparing these values with those of **1′**, it indicates that the two distinct reduction potentials observed for **1′** clearly correspond to the two stepwise reduction of BTDA-TCNQ.

Electron-filling of the BTDA-TCNQ units following Li-ion insertion was also confirmed by the infrared (IR) spectra. The stretching vibrational mode of the C≡N groups, observed at approximately 2200 cm^{-1}, was monitored in the pristine sample without Li-ion insertion (3.30 V vs. Li/Li^+) and in the Li-inserted cathode (2.72 V vs. Li/Li^+) (Figure 3c). The CN-stretching mode was observed as a multiplet, probably reflecting multiple coordination modes.[3,4,11] The characteristic peak at approximately 2230 cm^{-1} in the pristine cathode shifts to the lower wavenumber of 2200 cm^{-1} in the Li-inserted cathode. This shift is very similar to the variation observed in $BTDA\text{-}TCNQ^0$ (2232 cm^{-1}) and $K^+BTDA\text{-}TCNQ^-$ (2190 cm^{-1}), confirming that reduction of the BTDA-TCNQ moieties in $Li_x[\{Ru_2(2,3,5,6\text{-}F_4PhCO_2)_4\}_2(BTDA\text{-}TCNQ)]\cdot 2(p\text{-xylene})$ has occurred following Li-ion insertion. The red shifts of CN-stretching mode from the neutral state were also confirmed in further Li-inserted cathodes, although a distinct difference among them was not taken in the OCV range of 3.30–2.26 V (Supporting Information, Figure S8).

Figure 4 displays the temperature dependence of field-cooled magnetization (FCM at $H = 100$ Oe; closed circles) and remnant magnetization (open circles) of the Li-battery cell cathode at several selected OCVs. FCM of the pristine cathode without Li-ion insertion (3.30 V vs. Li/Li^+) showed paramagnetic behavior across the whole temperature range studied (down to 1.86 K), as observed in the bulk samples of **1′** (Supporting Information, Figure S5). When Li-ions and electrons were introduced into the cathode at 2.72 V vs. Li/Li^+, FCM showed a remarkable increase at temperatures below 40 K, and spontaneous magnetization was confirmed (field-dependence of the magnetization also showed an increase of the magnetization with a small hysteresis loop vs. the curve for the pristine **1′**; Supporting Information, Figure S9). This indicates that Li-ion insertion induces a long-range magnetic order in the magnetically disordered state of **1′** as a result of electron filling in the BTDA-TCNQ units. This magnetic feature should be due to ferrimagnetic ordering of the $S = 1$ spins of the $[Ru_2^{II,II}]$ units via the $S = 1/2$ spins of the electrochemically induced $BTDA\text{-}TCNQ^{\bullet -}$ units (Supporting Information, Figure S10), similar to that observed in $[FeCp^*_2][\{Ru_2(2,3,5,6\text{-}F_4PhCO_2)_4\}_2TCNQ]$.[4]

The magnetically ordered state is modulated by the quantity of inserted Li-ions/electrons, that is, the electron-filling level. As OCV decreases from 2.72 V to 2.38 V vs. Li/Li^+ (Figure 3a), the magnetic transition temperature (T_C) increases from 42 K to 88 K (Figure 4). The increase in T_C could be attributed to the growth of exchange-interacted-bond networks made by a $[\text{-}\{Ru_2^{II,II}\}\text{-}(BTDA\text{-}TCNQ^{\bullet -})\text{-}\{Ru_2^{II,II}\}\text{-}]$ repeat in a D_2A layer. Namely, magnetic pathways are developed to make growing domains when the BTDA-TCNQ units were reduced to yield $BTDA\text{-}TCNQ^{\bullet -}$ (Fig-

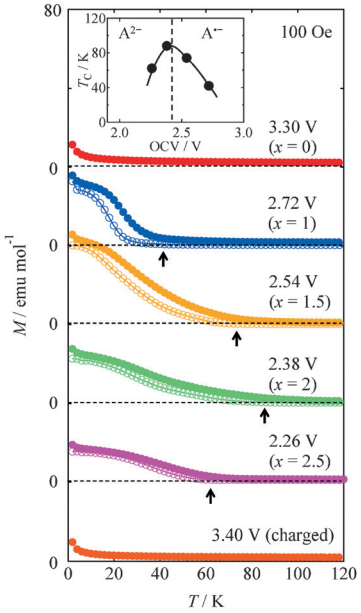

Figure 4. Temperature dependence of the cathode magnetization of $Li_x[\{Ru_2(2,3,5,6\text{-}F_4PhCO_2)_4\}_2(BTDA\text{-}TCNQ)]\cdot 2$ (*p*-xylene) at each equilibrium electrochemical potential vs. Li/Li^+ (OCV), where closed and open circles represent field-cooled and remnant magnetization, respectively, and the arrow represents T_C for each sample. The nominal Li-composition (x) per formula unit estimated from the discharged capacity, which includes the contribution from irreversible capacity of Li-battery cell, is displayed in addition to the OCV. The inset shows OCV dependence of T_C, where the dotted line is only a guide for the eye. $A^{\bullet-}$ (A^{2-}) represents BTDA-$TCNQ^{\bullet-}$ (BTDA-$TCNQ^{2-}$).

ure 1 b). Following this, BTDA-TCNQ finally undergoes two-electron reduction to form diamagnetic BTDA-$TCNQ^{2-}$. Hence, further insertion of Li-ions into the system beyond the threshold required for the complete production of BTDA-$TCNQ^{\bullet-}$, suppresses the occurrence of magnetic ordering. In this situation, the magnetically ordered state is destabilized because the production of BTDA-$TCNQ^{2-}$ cuts the exchange paths. In fact, when OCV is at 2.26 V vs. Li/Li^+, which is much lower than the second reduction peak of the BTDA-TCNQ unit, T_C decreases to 62 K (See the inset of Figure 4). The variation of T_C could be well explained by a simple mean-field model (Supporting Information, Figure S11).

Finally, charging the Li-battery cell returns the system to its original paramagnetic state (Figure 4). However, we also realized that repeated discharge/charge cycles resulted in damage to the sample as confirmed by capacity fading (Supporting Information, Figure S12). Therefore, based on the observed battery performance, the compound and/or the components of the battery system should be further improved for more effective magnetic control. Nevertheless, the present neutral D/A-MOF system is one of the most promising candidates for inclusion in a magnetic switchable battery. It should be noted that similar electron-filling-controlled magnetic behavior has also been confirmed by in situ magnetization measurement using a small Li-battery cell (Supporting Information, Figure S13).

In summary, we have succeeded in the artificial construction of a ferrimagnetically ordered state from a magnetically disordered ground state by electron-filling control of magnetic mediators (acceptor units) in a neutral D/A-MOF. This series of redox-active properties was designed on the basis of the frontier molecular orbital levels of donor and acceptor units through Li-ion insertion. This electrochemical approach, which is combined with ion insertion for the construction of magnetic correlations, may pave the way for the better design of molecular magnets based on redox-active MOFs.

Acknowledgements

We thank H. Fukunaga (Tohoku University) for his advice on regarding sample preparation and Dai-ichi Kogyo Seiyaku for the supply of ionic liquid. This work was supported by Grants-in-Aid for Scientific Research (nos. 15K13652, 26810029) and a Grant-in-Aid for Scientific Research on Innovative Areas ("π-System Figuration" Area 2601, no. 15H00983) and a MEXT program "Elements Strategy Initiative to Form Core Research Center" (since 2012) from the Ministry of Education, Culture, Sports, Science, and Technology, Japan, the E-IMR project, FRIS project, the Asahi Glass Foundation, and the Mitsubishi Foundation.

Keywords: donor–acceptor systems · electronic structure · lithium batteries · magnetic properties · metal–organic frameworks

How to cite: *Angew. Chem. Int. Ed.* **2016**, *55*, 5238–5242
Angew. Chem. **2016**, *128*, 5324–5328

[1] a) J. S. Miller, A. J. Epstein, *Angew. Chem. Int. Ed. Engl.* **1994**, *33*, 385; *Angew. Chem.* **1994**, *106*, 399; b) X.-Y. Wang, C. Avendaño, K. R. Dunbar, *Chem. Soc. Rev.* **2011**, *40*, 3213; c) J. S. Miller, *Chem. Soc. Rev.* **2011**, *40*, 3266.

[2] a) J. S. Miller, J. C. Calabrese, H. Rommelmann, S. R. Chittipeddi, J. H. Zhang, W. M. Reiff, A. J. Epstein, *J. Am. Chem. Soc.* **1987**, *109*, 769; b) W. E. Broderick, J. A. Thompson, E. P. Day, B. M. Hoffman, *Science* **1990**, *249*, 401; c) P.-M. Allemand, K. C. Khemani, A. Koch, G. Grüner, J. D. Thompson, *Science* **1991**, *253*, 301.

[3] a) H. Miyasaka, T. Izawa, N. Takahashi, M. Yamashita, K. R. Dunbar, *J. Am. Chem. Soc.* **2006**, *128*, 11358; b) N. Motokawa, H. Miyasaka, M. Yamashita, K. R. Dunbar, *Angew. Chem. Int. Ed.* **2008**, *47*, 7760; *Angew. Chem.* **2008**, *120*, 7874; c) N. Motokawa, T. Oyama, S. Matsunaga, H. Miyasaka, M. Yamashita, K. R. Dunbar, *CrystEngComm* **2009**, *11*, 2121; d) H. Miyasaka, N. Motokawa, S. Matsunaga, M. Yamashita, K. Sugimoto, T. Mori, N. Toyota, K. R. Dunbar, *J. Am. Chem. Soc.* **2010**, *132*, 1532; e) N. Motokawa, S. Matsunaga, S. Takaishi, H. Miyasaka, M. Yamashita, K. R. Dunbar, *J. Am. Chem. Soc.* **2010**, *132*, 11943; f) W. Kosaka, H. Fukunaga, H. Miyasaka, *Inorg. Chem.* **2015**, *54*, 10001.

[4] H. Fukunaga, H. Miyasaka, *Angew. Chem. Int. Ed.* **2015**, *54*, 569; *Angew. Chem.* **2015**, *127*, 579.

[5] a) G. Férey, F. Millange, M. Morcrette, C. Serre, M.-L. Doublet, J.-M. Grenèche, J.-M. Tarascon, *Angew. Chem. Int. Ed.* **2007**, *46*, 3259; *Angew. Chem.* **2007**, *119*, 3323; b) Z. Zhang, H. Yoshikawa, K. Awaga, *J. Am. Chem. Soc.* **2014**, *136*, 16112.

[6] a) O. Sato, T. Iyoda, A. Fujishima, K. Hashimoto, *Science* **1996**, *271*, 49; b) M. Okubo, D. Asakura, Y. Mizuno, T. Kudo, H. Zhou, A. Okazawa, N. Kojima, K. Ikeda, T. Mizokawa, I. Honma, *Angew. Chem. Int. Ed.* **2011**, *50*, 6269; *Angew. Chem.* **2011**, *123*,

6393; c) Y. Mizuno, M. Okubo, K. Kagesawa, D. Asakura, T. Kudo, H. Zhou, K. Oh-ishi, A. Okazawa, N. Kojima, *Inorg. Chem.* **2012**, *51*, 10311; d) T. Yamada, K. Morita, H. Wang, K. Kume, H. Yoshikawa, K. Awaga, *Angew. Chem. Int. Ed.* **2013**, *52*, 6238; *Angew. Chem.* **2013**, *125*, 6358; e) C. H. Li, M. K. Peprah, D. Asakura, E. Hosono, M. W. Meisel, M. Okubo, D. R. Talham, *Chem. Mater.* **2015**, *27*, 1524.

[7] M. Okubo, K. Kagesawa, Y. Mizuno, D. Asakura, E. Hosono, T. Kudo, H. Zhou, K. Fujii, H. Uekusa, S. Nishimura, A. Yamada, A. Okazawa, N. Kojima, *Inorg. Chem.* **2013**, *52*, 3772.

[8] a) V. Sivakumar, C. A. Ross, N. Yabuuchi, Y. Shao-Horn, K. Persson, G. Ceder, *J. Electrochem. Soc.* **2008**, *155*, 83; b) S. Dasgupta, B. Das, M. Knapp, R. A. Brand, H. Ehrenberg, R. Kruk, H. Hahn, *Adv. Mater.* **2014**, *26*, 4639; c) T. Yamada, K. Morita, K. Kume, H. Yoshikawa, K. Awaga, *J. Mater. Chem. C* **2014**, *2*, 5183.

[9] a) H. Miyasaka, *Acc. Chem. Res.* **2013**, *46*, 248.

[10] K. Nakabayashi, M. Nishio, K. Kubo, W. Kosaka, H. Miyasaka, *Dalton Trans.* **2012**, *41*, 6072.

[11] W. Kosaka, T. Morita, T. Yokoyama, J. Zhang, H. Miyasaka, *Inorg. Chem.* **2015**, *54*, 1518.

[12] H. Miyasaka, N. Motokawa, R. Atsuumi, H. Kamo, Y. Asai, M. Yamashita, *Dalton Trans.* **2011**, *40*, 673.

[13] W. Kosaka, M. Itoh, H. Miyasaka, *Dalton Trans.* **2015**, *44*, 8156.

[14] K. Nakabayashi, H. Miyasaka, *Chem. Eur. J.* **2014**, *20*, 5121.

[15] H. Matsumoto, H. Sakaebe, K. Tatsumi, M. Kikuta, E. Ishiko, M. Kono, *J. Power Sources* **2006**, *160*, 1308.

[16] W. Weppner, R. A. Huggins, *J. Electrochem. Soc.* **1977**, *124*, 1569.

[17] a) T. Ohzuku, M. Kitagawa, T. Hirai, *J. Electrochem. Soc.* **1990**, *137*, 769; b) S. Scharner, W. Weppner, P. Schmid-Beurmann, *J. Electrochem. Soc.* **1999**, *146*, 857; c) A. Yamada, H. Koizumi, S. Nishimura, N. Sonoyama, R. Kannno, M. Yonemura, T. Nakamura, Y. Kobayashi, *Nat. Mater.* **2006**, *5*, 357; d) Y. Gu, K. Taniguchi, R. Tajima, S. Nishimura, D. Hashizume, A. Yamada, H. Takagi, *J. Mater. Chem. A* **2013**, *1*, 6550.

[18] CCDC 1448623 (**1′**) and 1448624 (**1**) contain the supplementary crystallographic data for this paper. These data are provided free of charge by The Cambridge Crystallographic Data Centre.

Received: February 17, 2016
Published online: March 15, 2016

